AGRICULTURAL
SCIENCE & TECHNOLOGY

Open Access

Article

Rapid Tris(1,3-dichloropropyl) Phosphate Degradation and Detoxification via TiO_2 Nanoparticles under UV Light: Kinetics and Mechanism, Environmental Implications, and Insights into DFT

Ming Chang, Tesfaye Abebe Geleta, Hong-Jhang Chen, and Yang-hsin Shih*

ABSTRACT: The widespread use of tris(1,3-dichloropropyl) phosphate (TDCPP), a phosphorus flame retardant, has raised significant environmental concerns because of its persistence and toxicity. This study examines the photodegradation of TDCPP (0.25 mg/L) using titanium dioxide (TiO_2) nanoparticles (P25 NPs) (50 mg/L) under UV irradiation, focusing on the effects of electrolytes, such as NaCl and NaBr, pH, and temperature. TiO_2 NPs degraded TDCPP within 60 min, achieving nearly complete mineralization and release of chloride ions (Cl−). The degradation rate decreased with higher initial TDCPP concentrations but increased with higher TiO_2 dosages. Acidic conditions enhanced photodegradation, while the presence of electrolytes caused nanoparticle aggregation, increasing the particle size and reducing the photocatalytic efficiency. Chloride (Cl−) and bromide ions (Br−) acted as radical scavengers, inhibiting the formation of reactive hydroxyl radicals (HO•). Notably, 89% of the total organic carbon (TOC) was eliminated from TDCPP after 60 min of UV illumination, indicating mineralization into carbon dioxide and water. The degradation intermediates were analyzed using ultrahigh-performance liquid chromatography (UHPLC), and two byproducts were identified after 10 min of treatment. Acute and chronic toxicity analyses revealed that TDCPP's intermediates were nontoxic. Density functional theory (DFT) calculations provide insights into electronic structures and degradation pathways. This research contributes to strategies for mitigating the environmental impact of hazardous flame retardants such as TDCPP.

KEYWORDS: *titanium dioxide (TiO_2), tris(1,3-dichloropropyl) phosphate (TDCPP), electrolyte, toxicity, density functional theory*

1. INTRODUCTION

Agricultural water contamination by emerging pollutants, including phosphorus-based flame retardants (PFRs), has raised concerns about environmental and food safety.[1,2] Tris(1,3-dichloropropyl) phosphate (TDCPP) is a PFR containing halogens. The main function of PFRs is to protect or enhance the properties of plastics, textiles, and furniture. With the increasing replacement of brominated flame retardants (BFRs) in agricultural equipment, packaging materials, and food storage containers, TDCPP has become one of the most widely detected PFRs in environmental and food-related matrices. Studies have reported its presence in irrigation water, soil, and even agricultural produce, raising concerns about potential uptake by crops and subsequent entry into the food chain.[3−6] TDCPP replaces penta-BDE in flexible polyurethane foam[7] and is the most prevalent PFRs detected in baby products containing flexible polyurethane foam.[8] The United States Environmental Protection Agency estimated the annual production of TDCPP and triphenyl phosphate (TPP) in the United States to be between 10 and 50 million pounds per year in 2006.[9] TDCPP is a persistent organic pollutant that can leach from agricultural plastics and foams used in greenhouses, storage facilities, and irrigation systems.[10,11]

Because PFRs are not covalently bound to host materials, it is relatively easy for them to diffuse into the surroundings via volatilization, leaching, or abrasion. This widespread contamination poses risks to soil microbial communities, plant growth, and aquatic ecosystems, ultimately affecting agricultural productivity and food security. High doses of PFRs have been associated with adverse reproductive, neurological, and carcinogenic effects.[9] Owing to adverse biological effects, TDCPP was subject to a European Union risk assessment process under an Existing Substance Regulation (EEC 793/93) (Regulation 1993). Recently, TDCPP was shown to induce phenotypic alteration and thyroid hormone imbalance in zebrafish larvae, which resulted in behavioral abnormalities during zebrafish embryonic development.[12] This indicated that TDCPP exhibits neurodevelopmental toxicity. In addition, TDCPP has been detected in aquatic biota and humans at levels as high as ppm.[13] High exposure to TDCPP has been observed in infants; therefore, it is urgent to develop an efficient method for TDCPP removal.[14]

Given the urgent need for sustainable water purification strategies in agriculture, photocatalytic degradation[15−18] has emerged as a promising method for removing persistent contaminants such as TDCPP from irrigation water and wastewater. Titanium dioxide (TiO_2) is widely utilized as a photocatalyst due to its availability, low cost, nontoxicity,

Received: March 4, 2025
Revised: June 24, 2025
Accepted: June 25, 2025

chemical stability, and ability to degrade organic pollutants under UV light.[4,19−21] TiO_2 exists naturally in various crystal forms, including anatase, rutile, and brookite.[22−24] These different polymorphs exhibit distinct properties and play crucial roles in various applications, such as photocatalysis and solar cells. Among these, anatase is particularly effective in photocatalytic applications owing to its band gap and stability.[25] Rutile TiO_2 is also valuable because of its superior photocatalytic and electronic transport properties compared with anatase.[26] Brookite, another TiO_2 crystal form, has been studied less but is known to exhibit unique properties that may be advantageous for specific applications.[24] Studies have shown that the synthesis method can significantly affect the properties of these crystal forms.

A mixed phase called Degussa P25 grade (a mixture of 75% anatase and 25% rutile) offers better photodegradation efficiency than other forms of TiO_2.[23,27] Photoexcitation of semiconductors typically results in the creation of an electron−hole pair, situated at the conduction band (CB) and valence band (VB) edges, through exposure to UV light or sunlight, both of which possess energies greater than the bandgap energy of the material supposed to be a catalyst. Upon migration across the interface, these electron−hole pairs can facilitate the reduction and oxidation of organic compounds adsorbed on the surface. The reaction of this electron−hole pair with water, and/or with O_2, and/or with hydroxyl groups at the semiconductor surface generates high oxidant species, such as $HO^{\bullet}$ and peroxide radicals, which are capable of completely destroying organic compounds,[28] as shown in eqs 1−6. In these reactions, $HO^{\bullet}$ is generally considered to be the most significant species in the photocatalytic degradation of organic compounds.

$$TiO_2 + h\nu \rightarrow TiO_2(e^-, h^+) \quad (1)$$

$$TiO_2(h^+) + RX_{ads} \rightarrow TiO_2 + RX_{ads}^{\bullet+} \quad (2)$$

$$TiO_2(h^+) + H_2O_{ads} \rightarrow TiO_2 + OH_{ads}^{\bullet+} + H^+ \quad (3)$$

$$TiO_2(h^+) + OH_{ads}^- \rightarrow TiO_2 + OH_{ads}^{\bullet+} \quad (4)$$

$$TiO_2(e^-) + O_{2,ads} \rightarrow TiO_2 + O_2^{\bullet-} \quad (5)$$

$$TiO_2(e^-) + H_2O_{2,ads} \rightarrow TiO_2 + OH^- + OH_{ads}^{\bullet} \quad (6)$$

where RX_{ads} represents an organic molecule adsorbed onto the surface of TiO_2 and $RX_{ads}^{\cdot+}$ is the radical cation form of the organic molecule after it has lost an electron owing to the oxidation process.

In the environment, several factors—such as TDCPP concentration, P25 NP dosage, temperature, pH, and the presence of electrolytes (e.g., NaCl and NaBr)—influence the removal efficiency of contaminants by P25 NPs. These factors need to be systematically evaluated. When commercial TiO_2 enters water-containing electrolytes, it easily aggregates, and its particle size increases. As the electrostatic repulsion between two similarly charged surfaces decreases, particles can be bound together through attractive van der Waals forces.[29] In addition, TiO_2 aggregation also occurs at pH near the point of zero charge owing to the decrease in electrostatic repulsion. The photocatalytic activity of TiO_2 with NaCl decreases when the particle size increases from 244 to 13,000 nm.[30] The reduction of reactive oxygen species (ROS) generation when particles aggregate might result from reduced mass transfer and shadowing effects.[31] Several studies have discussed the effects of inorganic ions on the photocatalytic activity of TiO_2 and photocatalytic degradation efficiency of organic contaminants.[32−34] Furthermore, many researchers are focusing on using advanced oxidation processes (AOPs), like ozonation,[35] UV-based oxidation,[36,37] and electrochemical methods,[38] to remove stubborn organic pollutants. Among these, UV-driven AOPs stand out as a widely used and effective approach due to their high ability to break down various contaminants. UV/TiO_2 photocatalysis, a type of UV-AOP, involves light-induced excitation of semiconductor electrons, leading to the generation of nonselective reactive species (e.g., •OH), and has shown great potential for removing persistent organic pollutants.[39]

Many inorganic ions exhibit inhibitory effects, which can be attributed to two possible reasons. The first is competitive adsorption between the target compounds and inorganic ions at the active sites of TiO_2, which reduces the photocatalytic activity during the photocatalytic process. Second, inorganic ions might play the role of scavengers. They can react with photogenerated holes from TiO_2, thus reducing the number of oxidizing molecules required for the degradation of organic target compounds. Cl^- can compete with dichloroacetic acid for the TiO_2 adsorption sites. The adsorbed Cl^- sterically blocked the adsorption of dichloroacetic acid and inhibited the photocatalytic degradation efficiency.[40] In addition, some inorganic ions can produce byproducts during the photocatalytic process, which inhibits further degradation. Since there are electrolytes in the aquatic environment, the photodegradation of TDCPP by P25 NPs with two common anions, Cl^- or Br^-, needs to be understood.

This study aims to investigate the photocatalytic degradation of TDCPP using P25 NPs under UV irradiation, focusing on its potential application for agricultural water decontamination. The influence of key environmental factors, including the TDCPP concentration, TiO_2 nanoparticle dosage, temperature, pH, and presence of common electrolytes (NaCl and NaBr), was systematically examined. Understanding the role of electrolytes is particularly important for agricultural applications, as natural water sources used for irrigation often contain varying levels of salts that may affect photocatalytic efficiency. Furthermore, the degradation intermediates were identified, and their toxicity was assessed to evaluate potential risks in agricultural settings. Density functional theory (DFT) calculations were employed to provide molecular insights into TDCPP's degradation mechanisms.

By optimization of photocatalytic treatment conditions, this research provides a sustainable approach to mitigating the environmental risks posed by TDCPP in agricultural water systems. The findings contribute to the development of effective strategies for reducing flame retardant contamination in irrigation water, promoting safer food production, and improving overall environmental health.

2. MATERIALS AND METHODS

2.1. Materials. Tris(1,3-dichloro-2-propyl) phosphate ($C_9H_{15}C_{l6}O_4P$, >95%) was purchased from Tokyo Chemical Industry Co., Ltd. TiO_2 NPs (75% anatase and 25% rutile, denoted as P25 NPs) were purchased from Degussa (Evonik) Co., Ltd. Sodium chloride (NaCl, 99.5%), coumarin ($C_9H_6O_2$, ≥99%), coumarin-3-carboxylic acid (CCA, $C_{10}H_6O_4$, 98%), and sodium persulfate ($Na_2S_2O_8$,98%) were purchased from Acros Organics Co., Ltd. Hydrochloric acid (HCl, 36.5−38.0%), sodium hydroxide (NaOH, 98.7%), sodium bromide (NaBr, 99.5%), and phosphoric acid

(H_3PO_4, 85%) were obtained from J.T. Baker Co., Ltd. Potassium bromide (KBr, 99%) was purchased from Honeywell Fluka Co., Ltd. All solvents (hexane, methanol, and acetonitrile) of ultraresi-analyzed grade were purchased from Burdick and Jackson Co., Ltd.

All aqueous solutions were prepared by using deionized water with a Milli-Q water purification system (18.2 MΩ/cm, Millipore, Bedford, Massachusetts, USA). Stoke solutions were stored at 4 °C in the dark and allowed to reach room temperature before use. All of the experiments were performed at room temperature (25 ± 2 °C).

2.2. Experimental Procedures. Experiments were conducted in a photochemical reactor (PR-2000, Panchum Co., Ltd.) equipped with four 8 W UV lamps at an irradiation wavelength of 254 nm. The batch experiments were conducted in 15 mL transparent glass test tubes. The final concentrations were 0.25 mg/L TDCPP and 50 mg/L P25 NPs, in a total volume of 10 mL. The electrolyte contained NaCl and NaBr, with a concentration range of 0−500 mM. The photodegradation experiments were performed at room temperature. Prior to irradiation, the suspension was stirred in the dark for 30 min to achieve an adsorption−desorption equilibrium between TDCPP and P25 NPs. At the selected time intervals, 1 mL of the sample was removed, mixed with 3 mL of hexane, extracted using a vortex orbital mixer for 30 min, followed by centrifugation, and analyzed using a gas chromatograph (GC, Agilent 6890) equipped with an electron capture detector (ECD).

Ecological Structure Activity Relationships (ECOSAR) performs toxicity predictions based on the chemical structures of compounds. It utilizes quantitative structure−activity relationship (QSAR) models that correlate the chemical structure of TDCPP and its degradation intermediates with the biological activity. ECOSAR selects appropriate models based on the chemical's characteristics, focusing on aquatic acute toxicity end points such as lethal concentration (LC_{50}) and effective concentration (EC_{50}), as well as chronic toxicity values (ChV) for fish, daphnid, and green algae.

2.3. Characterization of P25 NPs. The surface area, pore size, and pore volume of P25 NPs with NaCl and NaBr were measured using the gas adsorption method Accelerated Surface Area and Porosimetry System (ASAP 2010, Micromeritics) and calculated using Brunauer−Emmett−Tetchel (BET, Beckman Coulter SA 3100) analysis. The size and zeta potential of the P25 NPs were analyzed by dynamic light scattering (DLS) using a zeta potential analyzer (Zetasizer, Nano ZS, Malvern, Massachusetts).

2.4. Aggregation and Sedimentation of P25 NPs. Batch experiments were performed to investigate the effects of different concentrations of electrolytes, including NaCl and NaBr, with TDCPP on the aggregation of P25 NPs using DLS. Sedimentation experiments via time-resolved optical absorbance of P25 NPs were performed by using an ultraviolet−visible spectrophotometer (UV−vis, UNICO) at 365 nm.

First, the P25 NP suspension was homogenized for 40 min by using an ultrasonic oscillator. Aggregation and sedimentation experiments were conducted by adding 5 mL of a 100 mg/L P25 NP suspension under different aquatic conditions into a test tube. To ensure even sampling, every tube was mixed in the initial setting and before the measurements. The suspension (3 mL) was transferred to a cuvette for aggregation experiments, and another 3 mL of the suspension was transferred to a quartz cuvette for sedimentation experiments. UV−vis absorbance measurements were carried out at room temperature.

2.5. Analytic Methods. After TDCPP extraction, the hexane extract phase of the TDCPP samples was placed into autosampler vials and analyzed by GC-ECD. The column was DB-5 (30 m × 0.32 mm) with a 0.25 mm film. The carrier gas was ultrahigh-purity N_2 (99.999%), with a flow rate of 7 mL/min. The injector temperature was 280 °C, and the oven temperature was 100 °C, ramped at 40 °C/min to 280 °C. The detector temperature was 280 °C. The retention time of TDCPP was in the range of 3.2−3.3 min.

The total organic carbon (TOC) in the water was measured using an Aurora Model 1030 W TOC analyzer with an Aurora Model 1088 autosampler. The principle of the analyzer operation was utilization of a sodium persulfate solution and heating to 98 °C to oxidize organic carbon. Samples contained 0.25 mg/L TDCPP and 5 mg/L P25 NPs with a total volume of 10 mL. During the analysis, the samples were acidized with 17% phosphoric acid (0.5 mL), sparged with nitrogen gas, and oxidized. Carbon dioxide formed during the oxidation process was subsequently quantified by using an infrared detector. Potassium hydrogen phthalate served as a standard for the development of the calibration curves.

The Cl^- in the solution was determined by ion chromatography (IC, Model 861 Advanced Compact IC, Switzerland). After photodegradation, 3 mL TDCPP samples were added to a 15 mL centrifuge tube, placed in an auto sampler, and analyzed by IC.

2.6. Measurements of Reactive Oxygen Species. In the field of photocatalytic activity, the determination of the ROS plays a crucial role in investigating the dominant ROS generated by the catalyst upon irradiation. To investigate the formation of •OH in the suspension during chemical degradation by P25 with or without electrolytes, coumarin as a fluorescent probe was added to the suspension under the same conditions. Coumarin is a poorly fluorescent molecule that is known to form fluorescent 7-hydroxy coumarin (7-HC) by reaction with •OH in aqueous solutions. Coumarin is a good $HO^•$ scavenger even at low concentrations.[41] Because coumarin carried no charge and was not adsorbed on the surface of TiO_2, it could detect only $HO^•$ in the suspension. On the other hand, because CCA possessed a −COOH group that could adsorb at the terminal −OH group of TiO_2, it could detect •OH near the TiO_2 surface.[42]

A 5 mg/L P25 suspension was added to a cuvette containing 0.1 mM coumarin or CCA. Using a JASCO FP-6500 spectrofluorometer, the fluorescence intensity was monitored at 453 nm with excitation at 332 nm for coumarin and at 445 nm with excitation at 340 nm for CCA. The fluorescence emission intensity was measured at time intervals of UV irradiation, which was the same as that in the photodegradation experiments.

2.7. Computational Details. DFT computations were performed using the hybrid functional B3LYP method.[43,44] The 6-311G(d,p) basis sets[45] were employed in the Gaussian 09 program to perform a thorough geometry optimization without symmetry constraints. The optimized structure was visualized using GaussView 5.0.8.[46] Additionally, the natural bond orbital analysis was used for population analysis at the B3LYP/6-311G(d,p) level of theory using the Gaussian 09 software package.

3. RESULTS AND DISCUSSION

3.1. Characterization of P25 NPs. The zeta potential was monitored as a function of pH, and the observed pH_{pzc} value was 6.7 for the P25 NPs (Figure S1). During the photodegradation experiments, the solution pH was less than 6.7, indicating that the surface of the P25 NPs remained positively charged. In the presence of NaCl or NaBr, the charges on the surfaces of the P25 NPs were reduced under acidic or alkaline conditions. Since the solution pH in our photodegradation experiments was slightly acidic, the positive charges on the surface of the P25 NPs decreased after NaCl or NaBr was added. Therefore, at pH less than pH_{pzc}, the surface groups of P25 NPs might be replaced by halide ions in the presence of Cl^- or Br^-. A previous report indicated that the positive charges on the surface of TiO_2 reduced in the acidic pH region in the presence of fluoride ions because the surface ≡Ti−OH_2^+ groups were replaced by ≡Ti−F species[47,33] Therefore, in this study, the surface of ≡Ti−OH_2^+ groups on P25 NPs might be replaced by ≡Ti−Cl or ≡Ti−Br in the presence of Cl− or Br−.

The surface area of the catalysts dominated the adsorption of the target compounds and affected the degradation rates. The specific surface area also influenced the distribution of active sites on the P25 NPs, which were related to the production of photogenerated electron−hole pairs and ROS. Table S1 lists the BET surface areas of the P25 NPs with

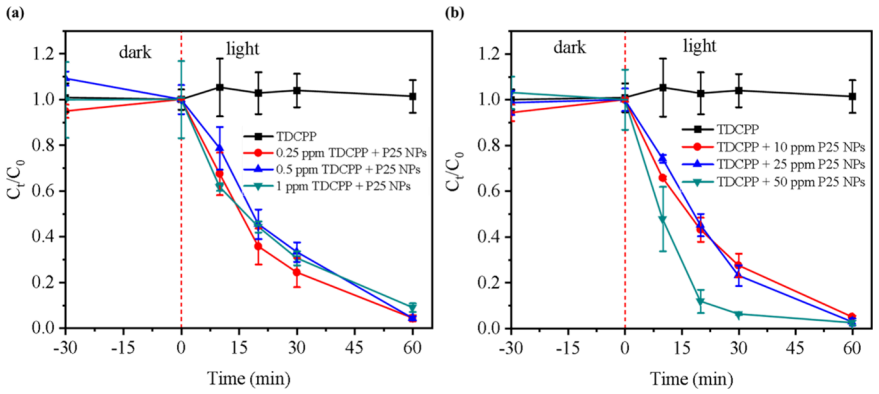

Figure 1. Photodegradation of TDCPP by P25 NPs: (a) at varying initial TDCPP concentrations using a fixed P25 NP dosage of 50 mg/L and (b) at different P25 NP dosages with a fixed initial TDCPP concentration of 0.25 mg/L under UV irradiation (8 W and λ = 254 nm).

Table 1. TDCPP Photodegradation Rate Constants and Correlation Coefficients of Different Initial TDCPP Concentrations and P25 NP Dosage

fixed parameter and concentration		variable parameter and concentration			
parameter	concentration (mg/L)	parameter	concentration (mg/L)	rate constant, k (min^{-1})	correlation coefficient, R^2
P25 NPs	50	TDCPP	0.25	0.0521	0.9955
			0.50	0.0514	0.9822
			1.00	0.0395	0.9985
TDCPP	0.25	P25 NPs	10	0.0493	0.9908
			25	0.0607	0.9830
			50	0.0613	0.9019

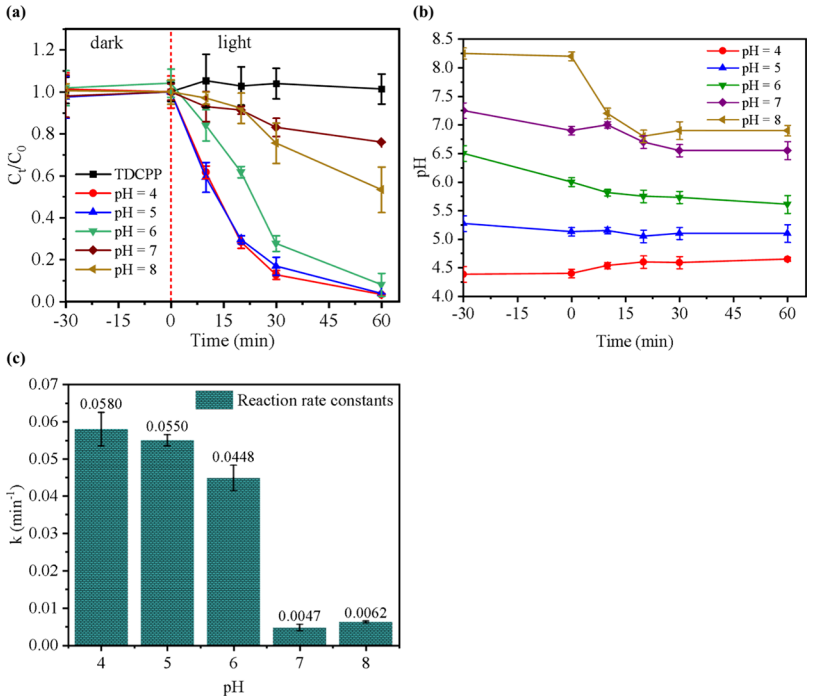

Figure 2. (a) Photodegradation of 0.25 mg/L TDCPP by 50 mg/L P25 NPs at different pH. (b) pH changes during the reactions of 0.25 mg/L TDCPP removal by 50 mg/L P25 NPs at different pH. (c) Relationship between initial pH and photodegradation reaction rate constants of 0.25 mg/L TDCPP with 50 mg/L P25 NPs.

different NaCl and NaBr concentrations. In the presence of Cl^- or Br^- ions, the specific surface area of the P25 NPs decreased with the electrolyte concentration, likely due to aggregation. Notably, when the salt/Ti ratio increased to more than 1.0, the specific surface area of TiO_2 was significantly decreased.[48]

3.2. Photocatalytic Degradation of TDCPP Using P25 NPs. *3.2.1. Effects of Initial TDCPP Concentrations and P25 NP Dosage.* The amount of organic compounds adsorbed on the catalyst surface may influence the removal efficiency.[49,50] However, Figure S2 shows that the TDCPP concentrations did not change significantly in the dark, indicating that TDCPP

Table 2. Comparison of TDCPP Degradation Using Different AOPs, Based on the Current Study and Previous Reports[a]

catalyst/anode	light source/current density	AOP method	oxidant/ozone dosage	TDCPP concentration (ppm)	rate constant (min^{-1})	reaction time (min)	degradation efficiency (%)	ref.
NA	UV lamp 20 W	UV/H2O2	0.5 mM H_2O_2	1	0.04919	60	95	54
Ti/SnO_2−Sb/La-PbO_2	10 mA/cm^2	EAOP	NA	1	0.0332	180	100	55
NA	UV lamp 8 W	UV/H_2O_2	20 mg/L	NA	NA	60	84	56
NA	UV lamp 8 W	UV/O_3	10 mg/L	NA	NA	120	30	56
P25 NPs (50 mg/L)	UV lamp 8 W	UV/P25	NA	0.25	0.0613	60	100	this study

[a]EAOPs: electrochemical advanced oxidation process; NA: non-available.

would not adsorb onto the P25 NP surface in 90 min. Therefore, we can conclude that the TDCPP concentration changes caused by adsorption onto the P25 NP surface during photodegradation can be ignored.

P25 NPs almost completely degraded TDCPP under UV irradiation within 60 min (Figure 1a). When the initial TDCPP concentrations (Figure 1b) were adjusted to 0.25 and 0.5 mg/L, P25 NPs almost completely degraded TDCPP in 60 min, whereas approximately 91% degradation was observed when the initial concentration was increased to 1.0 mg/L under the same conditions. The reaction rate constant (k) was calculated based on the entire degradation period using the pseudo-first-order kinetic model: $\ln(C_t/C_0) = -kt$. Here, C_0 and C_t represent the initial and final concentrations, respectively, and t is the irradiation time. However, the rate constants of the photodegradation of TDCPP by P25 NPs decreased when the initial TDCPP concentration increased (Table 1). On the other hand, the reaction rate constants increased with an increase in the P25 NP dosage from 10 to 50 mg/L (Figure 2b and Table 1). This concentration-dependent compound removal was also shown in several earlier studies under similar conditions, indicating that the rates of photodegradation of contaminants were strongly influenced by the number of active sites.[51−53] The rate constants of TDCPP degradation decreased owing to increasing competition with $HO^•$ radicals when the initial TDCPP concentrations were high. Increasing the P25 NP dosage resulted in more active sites for TDCPP, thus producing more $HO^•$, which could react with TDCPP more quickly.

A comparative evaluation of TDCPP degradation reveals notable differences in efficiency and kinetics across various AOP strategies, as shown in Table 2. The current study, employing UV/P25 TiO_2 photocatalysis, achieved complete degradation (100%) within 60 min at a low initial concentration (0.25 ppm), with the highest observed rate constant (0.0613 min^{-1}). In contrast, UV/H_2O_2 systems from previous studies required higher oxidant dosages and longer reaction times to achieve comparable or lower degradation efficiencies. Electrochemical AOPs (EAOPs), while achieving full removal, involved extended durations (up to 180 min), more complex setups (e.g., Ti/SnO_2−Sb/La−PbO_2 anodes), and higher current densities (10 mA/cm^2). Moreover, UV/O_3 demonstrated limited degradation (30%) over 120 min. These findings underscore the superior performance of UV/P25 in terms of both degradation rate and efficiency under mild conditions, highlighting its potential as a promising AOP for effective TDCPP removal.

3.3. Effects of Environmental Parameters on the Photocatalytic Degradation of TDCPP. *3.3.1. Effects of pH.* The effects of pH between 4 and 8 on the photodegradation of TDCPP by P25 NPs were investigated (Figure 2a). The solution pH was adjusted using 0.005 M HCl or 0.01 M NaOH. The amount of HCl used was minimal and consistent across all samples and did not significantly affect the total chloride concentration relative to the experimental NaCl levels. During the photodegradation process, the solution pH decreased, except at an initial pH of 4 (Figure 2b). After TDCPP photodegradation, TDCPP is mineralized to form CO_2 and water. When CO_2 dissolved in the suspension, it reacted with water to form HCO_3^- and H^+, leading to a decrease in the solution pH.

With an increase in pH, the photodegradation kinetics reaction slowed (Figure 2c and Table 3). When the solution pH was higher than 6, for pH_{zpc} of the P25 NPs, the photodegradation rates of TDCPP became significantly low. Because TDCPP is maintained in its molecular state without ionization under different pH conditions, the effects of pH variation on degradation mainly resulted from the characteristics of P25 NPs.

Table 3. Solution pH before and after Photodegradation of 0.25 mg/L TDCPP by 50 mg/L P25 NPs and the Reaction Rate Constants

adjusted pH	initial pH	final pH	rate constant, k (min^{-1})	correlation coefficient, R^2
4	4.38	4.65	0.058	0.9835
5	5.27	5.10	0.055	0.9950
6	6.50	5.61	0.045	0.9777
7	7.25	6.55	0.0047	0.9749
8	8.25	6.90	0.0062	0.9795

When the solution pH was lower than pH_{zpc}, the surface of the P25 NPs had a positive charge, which was more favorable for electrons to move from the VB to the CB. This is an essential process for the photocatalytic activity.[57] Therefore, the recombination of charge carriers was suppressed, resulting in more hole carriers in the VB (h_{vb}^+) reacting with OH^- adsorbed on the surface of the P25 NPs (OH_{ads}) to generate more $HO^•$ radicals.

3.3.2. Effects of Temperature. The effect of temperature on the photodegradation of TDCPP by P25 NPs was investigated between 15 and 35 °C (Figure S3). The rate constants increased with increasing temperature, which corresponds to general chemical reactions (Table S2). The k values were used to calculate the activation energy of the photodegradation of TDCPP using the Arrhenius equation (eq 7):[58]

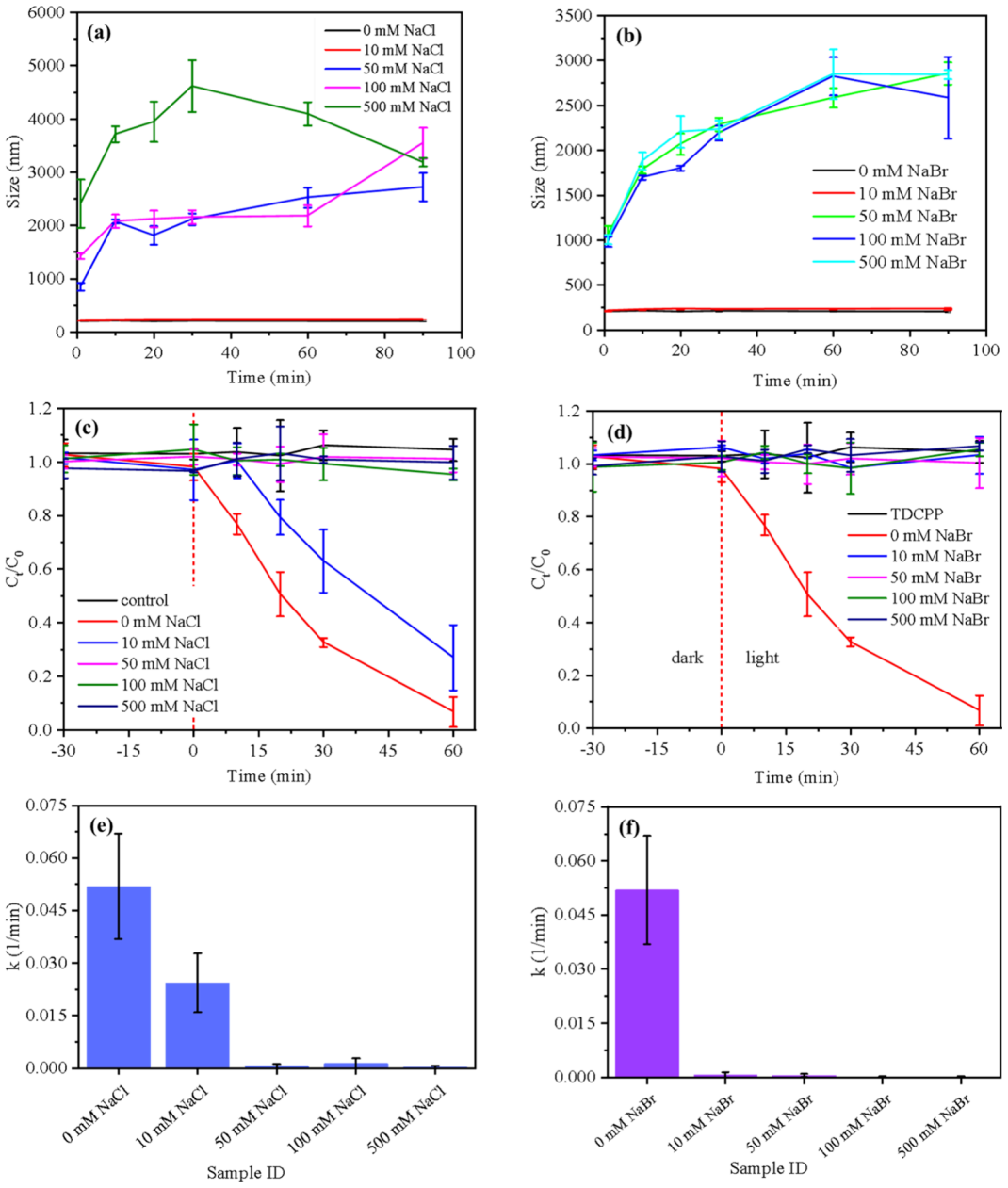

Figure 3. Influence of NaCl and NaBr concentrations on the photocatalytic degradation of TDCPP using P25 under 254 nm UV-light irradiation. (a, b) Particle size distribution of the reaction mixture at different concentrations of NaCl (a) and NaBr (b). (c, d) Photodegradation efficiency of TDCPP over time with varying concentrations of NaCl (c) and NaBr (d). (e, f) Pseudo-first-order rate constants corresponding to each salt concentration for NaCl (e) and NaBr (f). Reaction conditions: P25 = 50 mg/L; TDCPP = 0.25 mg/L; UV light (8 W and λ = 254 nm).

$$\ln k = \ln A - \frac{E_a}{RT} \quad (7)$$

where k is the rate constant of the pseudo-first-order model (min^{-1}), A is the Arrhenius coefficient, E_a is the activation energy (kJ/mol), R is the gas constant (8.314 J/mol·K), and T is the absolute temperature in kelvin (K). The activation energy was determined from the slope of the ln$k$ versus $1/T$ plot (Figure S4). The activation energy of the photodegradation of TDCPP by P25 NPs was 5.58 kJ/mol (R^2 = 0.949), which was relatively low.

3.3.3. Effects of Electrolytes. The P25 particles in this study did not disperse as primary particles but aggregated and became secondary particles. The aggregation kinetics and deposition behavior of TiO_2 NPs are rather complex processes that depend on the nature of the environmental conditions. The TiO_2 particle size plays an indispensable role in generating radicals because of the change in the total surface area, which is dependent on the presence of electrolytes. Therefore, it is important to observe the aggregation of P25 NPs over a wide range of electrolyte concentrations. NaCl and NaBr in this study are monovalent electrolytes in an environmental water matrix. The relationship between NaCl and NaBr concentrations and the P25 NP size is shown in Figure 3a and Figure 3b, respectively. The P25 NPs remained at approximately 200 nm without electrolytes for 90 min. The particle size increased from approximately 200 to approximately 3000 nm with over 50 mM NaCl or NaBr, owing to the aggregation of P25 NPs. The recorded average sizes of the P25 NP aggregates increased

continuously and quickly over time, indicating that aggregation occurred rapidly.

It has been reported that, in the presence of NaCl, the average hydrodynamic diameters of TiO_2 particles increased compared to the absence of NaCl,[30,59,60] which also indicated that the TiO_2 particle size increased with an increase in the concentration of NaBr.

The sedimentation kinetics of P25 NPs with TDCPP and 500 mM NaCl or NaBr are shown in Figure S5. The C_t/C_0 ratio of the P25 NP suspension in the DI water control (without electrolytes) did not change with time. The C_t/C_0 value of the P25 NP suspension with 500 mM NaCl or NaBr decreased quickly in 10 min, slowly in 30 min, and then became nearly steady in 90 min. This indicates that the P25 NPs aggregated to form stable aggregates and then settled with time with TDCPP and electrolytes.

The aggregation and sedimentation of the P25 NPs were attributed to the decrease in the surface potential on the P25 particle. In this study, because the pH of the P25 NP suspension was approximately 5 to neutral, the initial charges on the P25 NP surface were positive, and the negatively charged Cl^- or Br^- was easily adsorbed on the P25 surface through electrostatic interactions. Figure S1 presents the zeta potentials of the P25 NPs without electrolytes and in the presence of NaCl or NaBr. Without electrolytes, the P25 surface carries net positive charges under the original conditions and becomes less positive with increasing ionic strength (IS) because of the compression of the electric double layer (EDL).[61] An increase in IS of the aqueous system leads to a thinner EDL surrounding the NPs, which diminishes interparticle repulsion and promotes aggregation.[62] Therefore, the presence of electrolytes increases the rates of aggregation, size of the aggregates, and rates of sedimentation.[63−65]

The photodegradation of TDCPP by the P25 NP aggregates at different NaCl and NaBr concentrations was investigated under UV irradiation. The photodegradation kinetics of TDCPP by the P25 NP aggregates at different NaCl and NaBr concentrations are shown in Figure 3c and Figure 3d, respectively. In the absence of NaCl or NaBr, TDCPP was degraded by P25 NPs in 60 min. However, at different concentrations of NaCl and NaBr, the photodegradation of TDCPP by P25 NP aggregates was inhibited. Moreover, TDCPP was practically not degraded by P25 NP aggregates when NaCl was ≥50 mM or NaBr was ≥10 mM.

Pseudo-first-order kinetics was used to describe the photodegradation of TDCPP under UV light. The degradation rate constants decelerated with different concentrations of NaCl and NaBr, as shown in Figure 3e and Figure 3f, respectively. In the absence of electrolytes, TDCPP is degraded by $HO^•$ formed by the P25 NP aggregates under UV irradiation. However, with Cl^- or Br^-, they can compete with TDCPP for active sites,[66] react with $HO^•$ radicals as scavengers, and decrease the amount of $HO^•$ radicals.[67] Furthermore, the number of active sites on the surface of the P25 NP aggregates decreased as the P25 NPs aggregated, reducing the degradation rate constants. It has been reported that with an increase in the concentration of Cl^-, the photocatalytic degradation rate by TiO_2 nanotube films[68] or TiO_2 suspensions[69] is reduced.

The pH changes at the beginning and end (60 min) of the photoreactions with NaCl and NaBr are listed in Table S1. Regardless of whether NaCl or NaBr was added, the initial pH was around 5.4 to 5.9. The addition of NaCl resulted in only minor pH changes during the photodegradation process, with both initial and final pH values remaining nearly constant (≤0.04). However, the presence of NaBr led to a more pronounced increase in final pH, particularly at 50−100 mM, where the final pH rose by approximately ≤0.54, indicating a stronger influence of NaBr on the solution chemistry. Even though studies have pointed out that the yield of $HO^•$ production varied strongly with pH, the pH did not seem to be a main factor in the experiments because the pH at the initial and end of the experiments did not show obvious effects on the photodegradation rates.[70]

3.4. Mechanism. *3.4.1. Total Organic Compound Measurement.* To characterize the extent of mineralization of TDCPP, experiments were conducted by monitoring the changes in the total organic compounds (TOC). Under UV irradiation, the time-dependent TOC data of the TDCPP solution were measured with P25 NPs, as shown in Figure 4. It

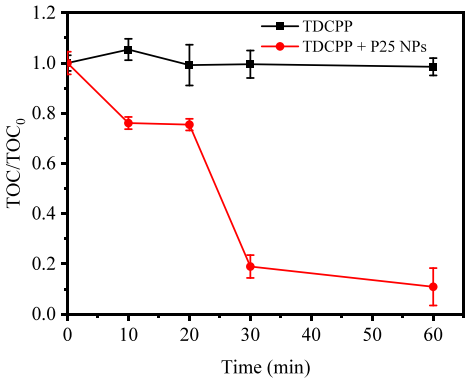

Figure 4. Time-dependent changes in total organic carbon (TOC) during the photodegradation of TDCPP under UV irradiation in the presence and absence of P25 NPs. Experimental conditions: [P25 NPs] = 50 mg/L, [TDCPP] = 0.25 mg/L, and UV lamps (8 W and λ = 254 nm).

was observed that 89% of the TOC was eliminated for TDCPP after 60 min of UV illumination, which suggested mineralization of TDCPP in the system to form carbon dioxide and water. The results indicated that most of the TDCPP was mineralized during the photocatalytic process, which is significant for practical applications of P25 NPs in photodegradation to avoid secondary pollution.

3.4.2. Chloride Ions Released from TDCPP. Cl^- was produced during the photodegradation process of 0.25 mg/L TDCPP by P25 NPs (Table 4). 0.25 mg/L TDCPP was equal to 0.58 μM of TDCPP, and one TDCPP molecule contained six chlorine atoms, so 3.48 μM Cl^- would be in the solution when all chlorine atoms from the TDCPP structure were released into the solution. When TDCPP was not degraded, 0.26−0.27 μM Cl^- was still present in the solution. The reason

Table 4. Chloride Ion Concentrations in 0.25 mg/L TDCPP Solution without and with 50 mg/L P25 NPs

	ion releasing concentration (μM)	
samples	Cl^-	PO_4^{3-}
TDCPP before UV irradiation	0.26	0.06
TDCPP after UV irradiation in 60 min	0.27	0.08
TDCPP+P25 after UV irradiation in 60 min	2.34	0.36

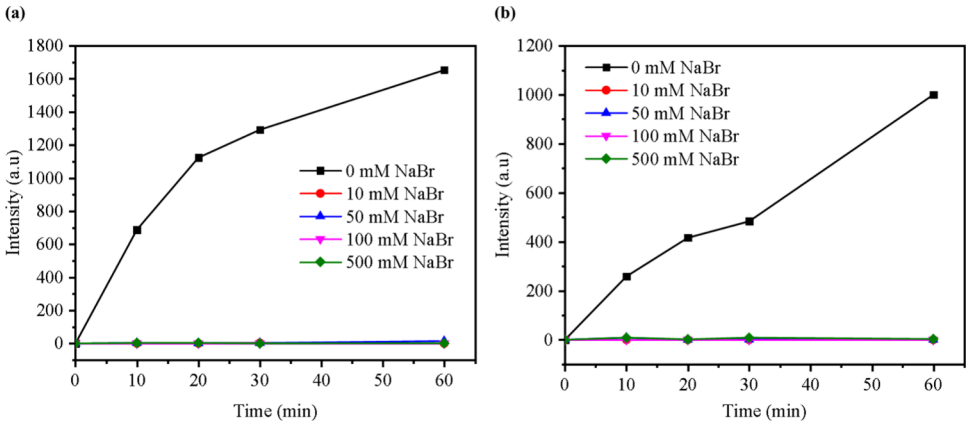

Figure 5. HO• produced by 50 mg/L P25 NP aggregates at different NaBr concentrations under UV irradiation (a) in a P25 NP suspension and (b) near a P25 NP surface.

might be that a few Cl^- ions existed in the TDCPP chemicals that we utilized. After the photocatalytic process for 60 min, approximately 2.08 μM Cl^- was released from TDCPP detected by IC, which means that approximately 60% of chlorine atoms from the TDCPP structure were released during the photodegradation process by the P25 NPs. Similar results were reported by another research group that investigated the photocatalytic degradation of other PFRs such as tris(1-chloro-2-propyl) phosphate (TCPP).[71]

3.4.3. Phosphate Ion Release from TDCPP. The release of phosphate ions (PO_4^{3-}) during the photocatalytic degradation of TDCPP was also monitored by using IC to evaluate the mineralization of its phosphorus-containing moiety. As shown in Table 3, the initial phosphate concentration in the 0.25 mg/L TDCPP solution was 0.06 μM under dark conditions, indicating trace impurities or minimal hydrolysis. UV irradiation alone led to a slight increase to 0.08 μM after 60 min, suggesting a limited contribution of photolysis to phosphate release. In contrast, the presence of 50 mg/L P25 NPs under UV irradiation after 60 min significantly increased the phosphate concentration to 0.36 μM, underscoring the catalytic role of P25 NPs in promoting TDCPP degradation. Given that 0.25 mg/L TDCPP corresponds to 0.58 μM, with one phosphorus atom per molecule, the observed phosphate release represents approximately 52% conversion of total phosphorus to the inorganic form. These results indicate that P25 NP-mediated photocatalysis effectively enhances the transformation of organically bound phosphorus, while the effect of UV light alone remains minimal.

3.4.4. Production of Hydroxyl Radicals. It is well-known that aromatic compounds are oxidized by HO• radicals much faster than by photogenerated holes in TiO_2 catalysts.[72] The generation of HO• radicals in the solution and near the P25 NP surface was investigated by using coumarin and CCA as fluorescent probes, respectively. Because CCA is more hydrophilic than coumarin, it is more likely to be adsorbed on the surface of P25 NPs, and thus, it can detect HO• radicals near the P25 NP surface.[42] In addition, the induction of fluorescence is mediated specifically by HO• radicals, which produce fluorescent hydroxyl products.

The relationship between the NaBr concentration and the amount of HO• generated by the P25 NP aggregates in the solution and near the P25 surface is illustrated in Figure 5a and Figure 5b, respectively. Gradual increases in the fluorescence at 453 and 445 nm with coumarin and CCA, both without NaBr, were observed with the UV irradiation time. However, in the presence of 10−500 mM NaBr, no HO• was detected. This means that the amount of generated HO• was not sufficient to react with coumarin or CCA and be detected by spectrofluorometry because less HO• was produced or the generated HO• was transformed in the photodegradation reactions.

The deceleration of the photodegradation rates of TDCPP by P25 NPs in the presence of NaCl or NaBr might result from a decrease in the surface area of P25 NPs, sedimentation of P25 NPs, and a reduced production of HO• radicals. However, the decrease in the surface area of the P25 NPs was not significant in the presence of 10 or 50 mM NaCl or NaBr. In contrast, the inhibition of TDCPP photodegradation was more pronounced with 50 mM NaCl, as well as with 10 and 50 mM NaBr. In addition, although approximately 50% of P25 NPs settled down in the presence of 500 mM NaCl or NaBr, TDCPP was still degraded by half dosages of P25 NPs, as shown in Figure S5; the P25 NPs could not completely degrade TDCPP with 500 mM NaCl or NaBr. Therefore, the decrease in the surface area of P25 NPs and sedimentation of P25 NPs might not be the main reason for the inhibition of photodegradation of TDCPP with NaCl or NaBr. Since HO• was the main radical for the destruction of contaminants during the photodegradation process and the production of HO• was eliminated significantly in the presence of NaBr, we believe that the reduced production of HO• was the main reason for the inhibition of the photodegradation of TDCPP with electrolytes.

3.5. TDCPP Degradation Intermediates and Density Functional Theory Analysis. The degradation intermediates of TDCPP ($C_9H_{15}Cl_6O_4P$) generated during the photocatalytic process were analyzed using the ultrahigh-performance liquid chromatography (UHPLC) system (Waters Corporation, Milford, Massachusetts) coupled with an Orbitrap Elite Hybrid Mass Spectrometer and Orbitrap Fusion Lumos Tribrid Mass Spectrometer (Thermo Fisher Scientific, Bremen, Germany). The analytical method was carried out by monitoring the degradation of TDCPP under UV irradiation at 10, 30, and 60 min. Aliquots from each reaction time were collected, combined into a single solution, and then filtered using a 0.22 μm PVDF membrane filter to remove the catalyst particles prior to analysis. The identification of degradation intermediates was subsequently performed using a UHPLC system. After 10 min of treatment, two primary intermediates, identified as TP313 ($C_6H_{10}Cl_3O_6P$) and TP207

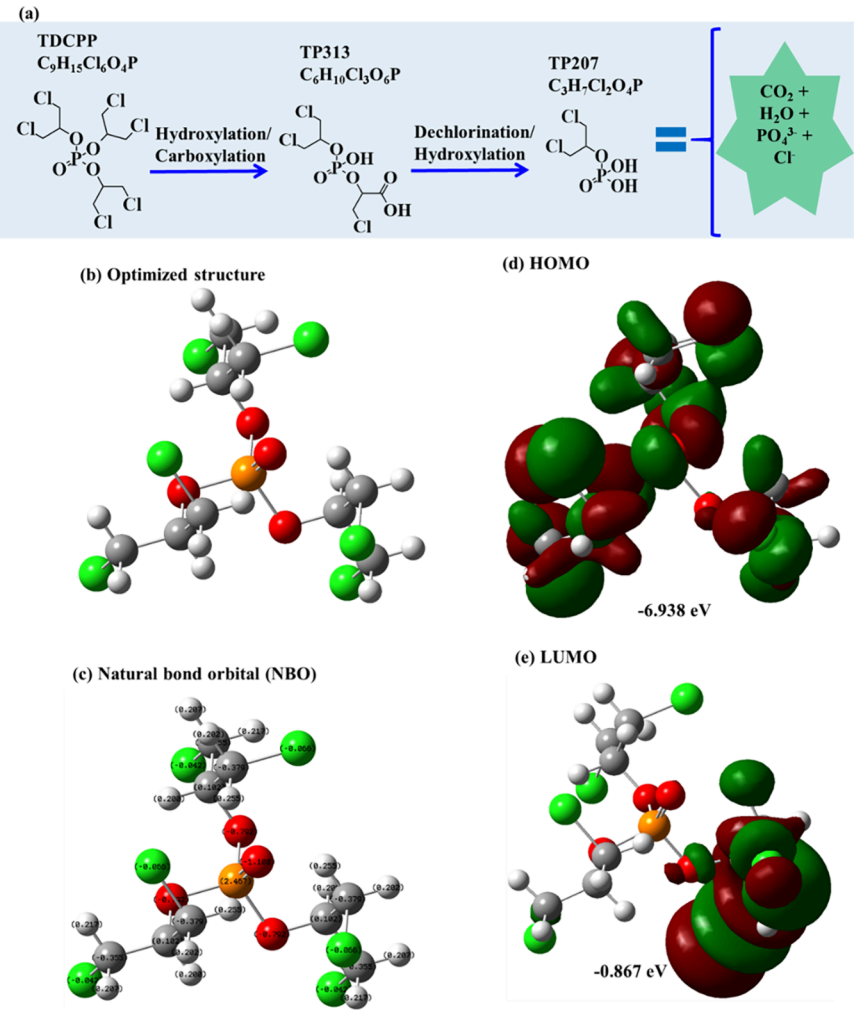

Figure 6. (a) Proposed degradation intermediate pathways of TDCPP using P25 as a catalyst under UV light and the DFT prediction of TDCPP molecular structure, including (b) optimized structure, (c) NBO, (d) HOMO), and (e) LUMO.

($C_3H_7Cl_2O_4P$), were detected. The proposed degradation pathways for these intermediates are illustrated in Figure 6a, with detailed MS information and isotopic patterns for TDCPP and its degradation intermediates presented in Figure S4. The degradation mechanism appears to proceed through an initial attack by $^{\bullet}OH$ on the $C_3H_5Cl_2-O$ and C−Cl bonds of TDCPP. This leads to oxidation reactions that facilitate the formation of a carboxylic acid group, resulting in the formation of intermediate TP313. Subsequently, TP313 undergoes dechlorination, followed by hydroxylation, to yield the second intermediate, TP207. This sequential degradation pathway highlights the critical role of hydroxyl radicals in breaking down TDCPP into progressively simpler intermediates via oxidation, dechlorination, and hydroxylation reactions. The analysis of TOC and Cl− concentrations during the degradation of TDCPP indicated that the final byproducts of this process are CO_2, H_2O, and Cl−. This finding confirms that TDCPP undergoes complete mineralization during degradation, resulting in nontoxic end products.

The degradation mechanism of TDCPP can be understood by examining its molecular orbital characteristics and comparing them with those of the observed intermediates, TP313 and TP207. Figure 6b shows the optimized molecular structure of TDCPP obtained by DFT calculations. This optimization minimizes the molecule's energy, revealing its most stable conformation. The optimized geometry serves as the foundation for further electronic structure analyses, including natural bond orbital (NBO) analyses, highest occupied molecular orbit (HOMO), and lowest unoccupied molecular orbit (LUMO) as shown in Figure 6c−e, helping to identify reactive sites and understand how TDCPP undergoes photocatalytic degradation.

NBO analysis further supports this by indicating a lower electron density or stability in these bonds, making them likely sites for hydrolysis or dechlorination (Figure 6c). The breakdown of TDCPP through these pathways highlights the relative weakness of the C−Cl and P═O bonds under oxidative conditions, as observed in other phosphate-based flame retardants.[73,74] The HOMO of TDCPP, concentrated around electronegative atoms like the phosphorus−oxygen (P═O) group and chlorine-substituted carbon atoms, indicates sites of high electron density that are more prone to oxidative attacks (Figure 6d). These regions, particularly the P═O group, may serve as initial targets for hydroxylation, consistent with the first transformation step leading to TP313 via hydroxylation and carboxylation.[75]

The LUMO analysis suggests areas that may be vulnerable to nucleophilic attacks, potentially facilitating bond cleavage or further transformation, especially near the P═O and C−Cl bonds (Figure 6e). This vulnerability aligns with the stepwise

Table 5. Estimation of Acute and Chronic Toxicity of TDCPP and Its Degradation Intermediates by Using the ECOSAR Predictive Model[a]

Chemicals	Acute toxicity (mg/L)			Chronic toxicity (mg/L)		
	Fish (LC_{50})	Daphnid (LC_{50})	Green Algae (EC_{50})	Fish (ChV)	Daphnid (ChV)	Green Algae (ChV)
TDCPP	5.26	10.9	3.99	0.42	2.02	1.42
TP313	39300	19800	8920	3330	1380	1780
TP207	2510	1260	574	213	88.3	115

[a]The toxicity values are classified into four grades: very toxic, $LC_{50}/EC_{50}/ChV \leq 1$, red label; toxic, $1 < LC_{50}/EC_{50}/ChV \leq 10$, orange label; harmful, $10 < LC_{50}/EC_{50}/ChV \leq 100$, yellow label; not harmful, $LC_{50}/EC_{50}/ChV > 100$, green label.

dechlorination observed in TDCPP's degradation pathway, where C−Cl bonds progressively break, leading to the formation of TP207.

Although photogenerated electrons (e−) in P25 NPs primarily reduce oxygen to form superoxide radicals, DFT analysis indicates that the HOMO of TDCPP is located on electron-rich sites (P═O and chlorinated carbons), which are highly susceptible to attack by electrophilic OH. These •OH radicals, generated from photogenerated holes in TiO_2, act as the main oxidizing agents for TDCPP. Direct electron transfer to TDCPP by photogenerated electrons is considered minimal.

Comparing the intermediates TP313 and TP207 with the DFT findings suggests a coherent mechanism: the electron-rich P═O bond initiates hydroxylation, while the less stable C−Cl bonds undergo sequential dechlorination. This degradation pathway illustrates how TDCPP's structural features, identified through molecular orbital analysis, determine its reactivity and susceptibility to environmental breakdown.[76] These insights not only elucidate the degradation process of TDCPP but also provide a foundation for predicting similar transformations in related compounds.

3.6. Toxicity of TDCPP. Using the ECOSAR predictive program, the structural data of TDCPP and its degradation products were analyzed to assess the toxicity levels. This assessment involved comparing TDCPP's acute and chronic toxicity against established toxic chemicals affecting fish, daphnid, and green algae.[15,55,77−79] An EC_{50} indicates the concentration needed to cause 50% mortality in green algae after 96 h, while LC_{50} denotes the concentration that results in 50% mortality in daphnids and fish after 48 and 96 h, respectively. The ChV reflect long-term cumulative effects of these chemicals in living organisms. Toxicity was categorized into four levels: very toxic (red label), toxic (orange label), harmful (yellow label), and not harmful (green label), as summarized in Table 5.

The acute LC_{50} to fish and daphnid were 5.26 and 10.9 mg/L for TDCPP, respectively, while it increased to 39,300 and 19,800 mg/L for TP313 and 2510 and 1260 for TP207, respectively. This indicated that the $C_3H_5Cl_2$−O bond substituted by an −OH bond would significantly reduce the toxicity. The EC_{50} for green algae was 3.99 mg/L for TDCPP, while it increased to 8920 mg/L for TP313 and 574 mg/L for TP207. Both intermediates exhibited a lower toxicity than TDCPP, leading to rapid detoxification during the photocatalytic reaction process.

For chronic toxicity, TDCPP also shows significant toxicity with ChV values of 0.42 mg/L for fish, 2.02 mg/L for daphnid, and 1.42 mg/L for green algae, maintaining its classification as "toxic". TP313 and TP207 display much lower chronic toxicity, with TP313 showing values of 3330 mg/L for fish, 1380 mg/L for daphnids, and 1780 mg/L for green algae, while TP207 has ChV values of 213 mg/L for fish, 88.3 mg/L for daphnid, and 115 mg/L for green algae, both remaining in the "not harmful" range. These results indicate that TDCPP is significantly more toxic in both acute and chronic exposure scenarios compared to its degradation intermediates. Overall, the data indicate that both TP313 and TP207 are significantly less toxic than TDCPP, demonstrating the effectiveness of the degradation process in mitigating the environmental risks associated with this flame retardant.

This study demonstrates the effective photocatalytic degradation of TDCPP using P25 NPs under UV irradiation. The degradation process achieved nearly complete removal of TDCPP within 60 min, accompanied by significant mineralization. However, the presence of common electrolytes, such as NaCl and NaBr, adversely affected photocatalytic performance due to nanoparticle aggregation, increased particle size, and radical scavenging effects, ultimately reducing the formation of reactive hydroxyl radicals (•OH). Degradation intermediates were identified and analyzed by using UHPLC and DFT simulations, which provided insights into the reaction pathways and structural vulnerability of TDCPP to oxidative attack. Toxicity analysis using the ECOSAR model confirmed that the transformation products were significantly less toxic than the parent compound, indicating effective detoxification during photocatalysis.

Overall, the photocatalytic degradation of TDCPP demonstrated an element-specific mineralization behavior. Approximately 89% of the total organic carbon was removed, indicating substantial oxidation of the carbon framework. Since the definition of mineralization is basically on the complete conversion to CO_2, TOC removal shows the real mineralization. The other elements could not be released from TDCPP or adsorbed or further converted by photocatalysts during the reactions.

These findings provide critical insights into the degradation behavior of halogenated organophosphorus flame retardants in aquatic environments and support the development of advanced photocatalytic systems for environmental remediation.

■ ASSOCIATED CONTENT

Supporting Information

The Supporting Information is available free of charge at https://pubs.acs.org/doi/10.1021/acsagscitech.5c00177.

(Figure S1) Zeta potentials of P25 NPs, P25 NPs + NaCl, and P25 NPs + NaBr ([P25 NPs] = 50 mg/L,

[NaCl] = 500 mM, and [NaBr] = 500 mM); (Figure S2) degradation of 0.25 mg/L TDCPP by 50 mg/L P25 NPs in the dark; (Figure S3) photodegradation of 0.25 mg/L TDCPP by 50 mg/L P25 NPs at different temperatures under UV light; (Figure S4) plot of ln k versus 1/T; (Figure S5) sedimentation kinetics of P25 NPs (50 mg/L) with TDCPP (0.25 mg/L) and 500 mM NaCl or 500 mM NaBr; (Figure S6) MS information and isotopic patterns of (a) TDCPP and its degradation intermediates, (b) TP313, and (c) TP207; (Table S1) solution pH before and after photodegradation of TDCPP (0.25 mg/L) by P25 (50 mg/L) NPs with different concentrations of NaCl and NaBr along the corresponding BET specific surface area and reaction rate constants; and (Table S2) photodegradation rate constants and the correlation coefficient of 0.25 mg/L TDCPP with 50 mg/L P25 NPs at different temperatures (PDF)

AUTHOR INFORMATION

Corresponding Author

Yang-hsin Shih − *Department of Agricultural Chemistry, National Taiwan University, Taipei 106, Taiwan;* orcid.org/0000-0002-1326-0720; Phone: 886-2-33669443; Email: yhs@ntu.edu.tw

Authors

Ming Chang − *Department of Agricultural Chemistry, National Taiwan University, Taipei 106, Taiwan*

Tesfaye Abebe Geleta − *Department of Agricultural Chemistry, National Taiwan University, Taipei 106, Taiwan;* orcid.org/0000-0002-6972-5881

Hong-Jhang Chen − *Institute of Food Science and Technology, National Taiwan University, Taipei 106, Taiwan;* orcid.org/0000-0002-9420-0964

Complete contact information is available at: https://pubs.acs.org/10.1021/acsagscitech.5c00177

Author Contributions

M. Chang: investigation, methodology, data curation, data analysis, and writing—original draft; T.A. Geleta: investigation, methodology, data curation, data analysis, writing—original draft, and writing—review and editing; H.-J. Chen: resources, data curation, investigation, writing—review, and editing; Y.-h. Shih: conceptualization, funding acquisition, project administration, resources, supervision, writing—review, and editing.

Notes

The authors declare no competing financial interest.

ACKNOWLEDGMENTS

We gratefully acknowledge financial support from the National Science and Technology Council of Taiwan, Republic of China (111-2221-E-002-084-MY3). The authors thank Ms. Gui-Ru Xie for her professional assistance with high-resolution mass spectrometry measurement. The authors also acknowledge the high-performance computing facilities at NTU.

REFERENCES

(1) Li, C.; Li, G. Impact of China's water pollution on agricultural economic growth: An empirical analysis based on a dynamic spatial panel lag model. *environmental science and pollution research* **2021**, *28* (6), 6956−6965.

(2) Ncibi, M. C.; Mahjoub, B.; Mahjoub, O.; Sillanpää, M. Remediation of emerging pollutants in contaminated wastewater and aquatic environments: biomass-based technologies. *Clean:Soil, Air, Water* **2017**, *45* (5), No. 1700101.

(3) Wang, X.; Song, F. The neurotoxicity of organophosphorus flame retardant tris (1, 3-dichloro-2-propyl) phosphate (TDCPP): Main effects and its underlying mechanisms. *Environ. Pollut.* **2024**, *346*, No. 123569.

(4) Wang, L.; Wang, B.; Zhang, X.; Yang, Z.; Zhang, X.; Gong, H.; Song, Y.; Zhang, K.; Sun, M. TDCPP and TiO2 NPs aggregates synergistically induce SH-SY5Y cell neurotoxicity by excessive mitochondrial fission and mitophagy inhibition. *Environ. Pollut.* **2024**, *347*, No. 123740.

(5) Picó, Y.; Campo, J.; Alfarhan, A. H.; El-Sheikh, M. A.; Barceló, D. A reconnaissance study of pharmaceuticals, pesticides, perfluoroalkyl substances and organophosphorus flame retardants in the aquatic environment, wild plants and vegetables of two Saudi Arabia urban areas: Environmental and human health risk assessment. *Sci. Total Environ.* **2021**, *776*, No. 145843.

(6) Poma, G.; Sales, C.; Bruyland, B.; Christia, C.; Goscinny, S.; Van Loco, J.; Covaci, A. Occurrence of organophosphorus flame retardants and plasticizers (PFRs) in Belgian foodstuffs and estimation of the dietary exposure of the adult population. *Environ. Sci. Technol.* **2018**, *52* (4), 2331−2338.

(7) Wang, C.; Chen, H.; Li, H.; Yu, J.; Wang, X.; Liu, Y. Review of emerging contaminant tris(1,3-dichloro-2-propyl)phosphate: Environmental occurrence, exposure, and risks to organisms and human health. *Environ. Int.* **2020**, *143*, No. 105946.

(8) Stapleton, H. M.; Misenheimer, J.; Hoffman, K.; Webster, T. F. Flame retardant associations between children's handwipes and house dust. *Chemosphere* **2014**, *116*, 54−60.

(9) Meeker, J. D.; Stapleton, H. M. House dust concentrations of organophosphate flame retardants in relation to hormone levels and semen quality parameters. *Environ. Health Perspect.* **2010**, *118* (3), 318−323.

(10) Salthammer, T.; Fuhrmann, F.; Uhde, E. Flame retardants in the indoor environment–Part II: release of VOCs (triethylphosphate and halogenated degradation products) from polyurethane. *Indoor Air* **2003**, *13* (1), 49−52.

(11) Saquib, Q.; Al-Salem, A. M.; Siddiqui, M. A.; Ansari, S. M.; Zhang, X.; Al-Khedhairy, A. A. Organophosphorus flame retardant TDCPP displays genotoxic and carcinogenic risks in human liver cells. *Cells* **2022**, *11* (2), 195.

(12) Xu, Y.; Yang, L.; Teng, Y.; Li, J.; Li, N. Exploring the underlying molecular mechanism of tri (1, 3-dichloropropyl) phosphate-induced neurodevelopmental toxicity via thyroid hormone disruption in zebrafish by multi-omics analysis. *Aquatic Toxicology* **2023**, *258*, No. 106510.

(13) Sundkvist, A. M.; Olofsson, U.; Haglund, P. Organophosphorus flame retardants and plasticizers in marine and fresh water biota and in human milk. *Journal of environmental monitoring* **2010**, *12* (4), 943−951.

(14) Hoffman, K.; Butt, C. M.; Chen, A.; Limkakeng, A. T., Jr; Stapleton, H. M. High exposure to organophosphate flame retardants in infants: associations with baby products. *Environ. Sci. Technol.* **2015**, *49* (24), 14554−14559.

(15) Huang, S.-E.; Tan, K.-H.; Sahu, R. S.; Geleta, T. A.; Miri, A.; Lin, C.-Y.; Shih, Y.-H.; Chen, W.-L. Facile Synthesis and Optimization of Graphitic Carbon Nitride Nanoparticles to Effectively Photodegrade Tetracycline under Visible Light in Water. *ACS Agricultural Science & Technology* **2025**, *5* (2), 235−245.

(16) Lin, F.-Y.; Lien, H.-L.; Shih, Y.-H.; Ta Fu Kuo, D. Effect of surfactants and implementation strategies for the pentachlorophenol degradation with Ni/Fe bimetallic nanoparticles in soil. *Sep. Purif. Technol.* **2025**, *354*, No. 129097.

(17) Lin, F.-Y.; Lien, H.-L.; Kuo, D. T. F.; Wang, K.; Shih, Y.-H. Degradation of Pentachlorophenol by CTAB-Modified Ni/Fe Bimetallic Nanoparticles in the Soil Solution. *ACS ES&T Engineering* **2024**, *4* (2), 318−329.

(18) Tan, K.-H.; Shih, Y.-h.; Chen, W.-L. Facile preparation of environmental benign LED white light active humic acid nanolayer coated titanium dioxide photocatalyst for bisphenol A degradation. *Chemosphere* **2024**, *355*, No. 141710.
(19) Wu, X.; Zhou, J.; Tan, Q.; Li, K.; Li, Q.; Correia Carabineiro, S. A.; Lv, K. Remarkable Enhancement of Photocatalytic Activity of High-Energy TiO2 Nanocrystals for NO Oxidation through Surface Defluorination. *ACS Appl. Mater. Interfaces* **2024**, *16*, 11479−11488.
(20) Abdullah, A. M.; O'Shea, K. E. TiO2 photocatalytic degradation of the flame retardant tris (2-chloroethyl) phosphate (TCEP) in aqueous solution: A detailed kinetic and mechanistic study. *J. Photochem. Photobiol., A* **2019**, *377*, 130−137.
(21) Huang, L.; He, G.; Yuan, Y.; Zhang, T. C.; Wang, Y.; Yuan, S. Trivalent Metal Ions (Al, Ga, In)-Doped TiO2 for Enhanced Photocatalytic Desulfurization of H2S: Band Structure Regulation, Performance, and Mechanism. *Ind. Eng. Chem. Res.* **2024**, *63* (16), 7154−7165.
(22) Eddy, D. R.; Permana, M. D.; Sakti, L. K.; Sheha, G. A. N.; Solihudin; Hidayat, S.; Takei, T.; Kumada, N.; Rahayu, I. Heterophase polymorph of TiO_2 (anatase, rutile, brookite, TiO_2 (B)) for efficient photocatalyst: fabrication and activity. *Nanomaterials* **2023**, *13*, 704.
(23) Al-Attafi, K.; Dwech, M. H.; Mezher, H. A.; Nattestad, A.; Kim, J. H. A Comparative Study of Organic Dye-Sensitized Solar Cells Based on Anatase TiO_2 and Amorphous Free Mixed Phase's Anatase/Rutile P25 TiO_2 Photoanodes. *Coatings* **2023**, *13* (1), 121.
(24) Nguyen, T. T.; Edalati, K. Brookite TiO_2 as an active photocatalyst for photoconversion of plastic wastes to acetic acid and simultaneous hydrogen production: Comparison with anatase and rutile. *Chemosphere* **2024**, *355*, No. 141785.
(25) Kusior, A.; Jeleń, P.; Sitarz, M.; Świerczek, K.; Radecka, M. 3D Flower-like TiO2 Nanostructures: Anatase-To-Rutile Phase Transformation and Photoelectrochemical Application. *Catalysts* **2023**, *13* (4), 671.
(26) Chen, B.; Kang, K.; Jeen, H.; Zhang, Y.; Lin, J.; Feng, B.; Ikuhara, Y.; Hoshino, S.; Matsunaga, K.; Ohta, H. Orthorhombic distortion-induced anatase-like optoelectronic properties of rutile TiO2. *J. Appl. Phys.* **2022**, *132* (18), No. 185301.
(27) Hurum, D. C.; Agrios, A. G.; Gray, K. A.; Rajh, T.; Thurnauer, M. C. Explaining the enhanced photocatalytic activity of Degussa P25 mixed-phase TiO2 using EPR. *J. Phys. Chem. B* **2003**, *107* (19), 4545−4549.
(28) Nasikhudin; Diantoro, M.; Kusumaatmaja, A.; Triyana, K. In *Study on photocatalytic properties of TiO2 nanoparticle in various pH condition*; IOP Publishing, 2018 p. 012069.
(29) Elimelech, M.; Gregory, J.; Jia, X. *Particle deposition and aggregation: measurement, modelling and simulation*; Butterworth-Heinemann, 2013.
(30) Shih, Y.-h.; Lin, C.-h. Effect of particle size of titanium dioxide nanoparticle aggregates on the degradation of one azo dye. *Environ. Sci. Pollut. Res. Int.* **2012**, *19*, 1652−1658.
(31) Hotze, E. M.; Bottero, J.-Y.; Wiesner, M. R. Theoretical framework for nanoparticle reactivity as a function of aggregation state. *Langmuir* **2010**, *26* (13), 11170−11175.
(32) Yuan, R.; Fan, S.; Zhou, H.; Ding, Z.; Lin, S.; Li, Z.; Zhang, Z.; Xu, C.; Wu, L.; Wang, X. Chlorine-Radical-Mediated Photocatalytic Activation of C-H Bonds with Visible Light. *Angew. Chem.* **2013**, *125*, 1069.
(33) Zhang, W.; An, T.; Cui, M.; Sheng, G.; Fu, J. Effects of anions on the photocatalytic and photoelectrocatalytic degradation of reactive dye in a packed-bed reactor. *Journal of Chemical Technology & Biotechnology: International Research in Process, Environmental & Clean Technology* **2005**, *80* (2), 223−229.
(34) Kashif, N.; Ouyang, F. Parameters effect on heterogeneous photocatalysed degradation of phenol in aqueous dispersion of TiO2. *Journal of Environmental Sciences* **2009**, *21* (4), 527−533.
(35) Gounden, A. N.; Singh, S.; Jonnalagadda, S. B. Simultaneous removal of 2, 4, 6-tribromophenol from water and bromate ion minimization by ozonation. *Journal of Hazardous Materials* **2018**, *357*, 415−423.
(36) Yin, K.; Deng, Y.; Liu, C.; He, Q.; Wei, Y.; Chen, S.; Liu, T.; Luo, S. Kinetics, pathways and toxicity evaluation of neonicotinoid insecticides degradation via UV/chlorine process. *Chemical Engineering Journal* **2018**, *346*, 298−306.
(37) Yuan, X.; Jiang, L.; Chen, X.; Leng, L.; Wang, H.; Wu, Z.; Xiong, T.; Liang, J.; Zeng, G. Highly efficient visible-light-induced photoactivity of Z-scheme Ag 2 CO 3/Ag/WO 3 photocatalysts for organic pollutant degradation. *Environmental Science: Nano* **2017**, *4* (11), 2175−2185.
(38) Yao, Y.; Huang, C.; Yang, Y.; Li, M.; Ren, B. Electrochemical removal of thiamethoxam using three-dimensional porous PbO2-CeO2 composite electrode: Electrode characterization, operational parameters optimization and degradation pathways. *Chemical Engineering Journal* **2018**, *350*, 960−970.
(39) Alvarez-Corena, J. R.; Bergendahl, J. A.; Hart, F. L. Photocatalytic Oxidation of Five Contaminants of Emerging Concern by UV/TiO2: Identification of Intermediates and Degradation Pathways. *Environmental Engineering Science* **2016**, *33* (2), 140−147.
(40) Krivec, M.; Dillert, R.; Bahnemann, D. W.; Mehle, A.; Štrancar, J.; Dražić, G. The nature of chlorine-inhibition of photocatalytic degradation of dichloroacetic acid in a TiO 2-based microreactor. *Phys. Chem. Chem. Phys.* **2014**, *16* (28), 14867−14873.
(41) Louit, G.; Foley, S.; Cabillic, J.; Coffigny, H.; Taran, F.; Valleix, A.; Renault, J. P.; Pin, S. The reaction of coumarin with the OH radical revisited: hydroxylation product analysis determined by fluorescence and chromatography. *Radiat. Phys. Chem.* **2005**, *72* (2−3), 119−124.
(42) Zhang, J.; Nosaka, Y. Mechanism of the OH radical generation in photocatalysis with TiO2 of different crystalline types. *J. Phys. Chem. C* **2014**, *118* (20), 10824−10832.
(43) Becke, A. D. A new mixing of Hartree−Fock and local density-functional theories. *J. Chem. Phys.* **1993**, *98* (2), 1372−1377.
(44) Halim, S. A.; El-Meligy, A. B.; El-Nahas, A. M.; El-Demerdash, S. H. DFT study, and natural bond orbital (NBO) population analysis of 2-(2-Hydroxyphenyl)-1-azaazulene tautomers and their mercapto analouges. *Sci. Rep.* **2024**, *14* (1), 219.
(45) Lee, C.; Yang, W.; Parr, R. G. Development of the Colle-Salvetti correlation-energy formula into a functional of the electron density. *Phys. Rev. B* **1988**, *37* (2), 785.
(46) Frisch, M.; Trucks, G. W.; Schlegel, H. B.; Scuseria, G. E.; Robb, M. A.; Cheeseman, J. R.; Scalmani, G.; Barone, V.; Mennucci, B.; Petersson, G. A. *gaussian 09*; Gaussian. Inc.: Wallingford CT, 2009, *121*, 150−166.
(47) Mrowetz, M.; Selli, E. H 2 O 2 evolution during the photocatalytic degradation of organic molecules on fluorinated TiO 2. *New J. Chem.* **2006**, *30* (1), 108−114.
(48) Chang, S.-m.; Lee, C.-y. A salt-assisted approach for the pore-size-tailoring of the ionic-liquid-templated TiO2 photocatalysts exhibiting high activity. *Appl. Catal., B* **2013**, *132*, 219−228.
(49) Naghdi, S.; Shahrestani, M. M.; Zendehbad, M.; Djahaniani, H.; Kazemian, H.; Eder, D. Recent advances in application of metal-organic frameworks (MOFs) as adsorbent and catalyst in removal of persistent organic pollutants (POPs). *J. Hazard. Mater.* **2023**, *442*, No. 130127.
(50) Šojić, D. V.; Orčić, D. Z.; Četojević-Simin, D. D.; Despotović, V. N.; Abramović, B. F. Kinetics and the mechanism of the photocatalytic degradation of mesotrione in aqueous suspension and toxicity of its degradation mixtures. *J. Mol. Catal. A: Chem.* **2014**, *392*, 67−75.
(51) Chiou, C.-H.; Wu, C.-Y.; Juang, R.-S. Influence of operating parameters on photocatalytic degradation of phenol in UV/TiO2 process. *Chem. Eng. J.* **2008**, *139* (2), 322−329.
(52) Hu, Q.; Zhang, C.; Wang, Z.; Chen, Y.; Mao, K.; Zhang, X.; Xiong, Y.; Zhu, M. Photodegradation of methyl tert-butyl ether (MTBE) by UV/H2O2 and UV/TiO2. *J. Hazard. Mater.* **2008**, *154* (1−3), 795−803.

(53) Tsai, W.-T.; Lee, M.-K.; Su, T.-Y.; Chang, Y.-M. Photodegradation of bisphenol-A in a batch TiO2 suspension reactor. *J. Hazard. Mater.* **2009**, *168* (1), 269−275.
(54) Luo, Z.; Yuan, L.; Wong, J. W. C.; Zhu, M.; Yu, Y.; Wang, K.; Yin, H.; Tang, S.; Niu, J. Degradation of tris (1, 3-dichloro-2-propyl) phosphate (TDCPP) by ultraviolet activated hydrogen peroxide: Mechanisms, pathways and toxicity assessments. *Chemical Engineering Journal* **2024**, *497*, No. 155690.
(55) Tang, S.; Luo, Z.; Liao, J.; Liu, Z.; Xu, L.; Niu, J. Degradation and detoxification mechanisms of organophosphorus flame retardant tris (1, 3-dichloro-2-propyl) phosphate (TDCPP) during electrochemical oxidation process. *Chin. Chem. Lett.* **2023**, *34* (8), No. 108090.
(56) Yuan, X.; Lacorte, S.; Cristale, J.; Dantas, R. F.; Sans, C.; Esplugas, S.; Qiang, Z. Removal of organophosphate esters from municipal secondary effluent by ozone and UV/H2O2 treatments. *Sep. Purif. Technol.* **2015**, *156*, 1028−1034.
(57) Bahnemann, D. W. Ultrasmall metal oxide particles: preparation, photophysical characterization, and photocatalytic properties. *Isr. J. Chem.* **1993**, *33* (1), 115−136.
(58) Liang, H.; Rehan, M. A.; Li, J.; Du, S.; Zhai, Y.; Li, G. Kinetic simulation of hydrogen production reaction parameters based on TiO2 photocatalyst. *Applied Thermal Engineering* **2024**, *239*, No. 122134.
(59) Muthukumaran, S.; Song, L.; Zhu, B.; Myat, D.; Chen, J.-Y.; Gray, S.; Duke, M. UV/TiO2 photocatalytic oxidation of recalcitrant organic matter: effect of salinity and pH. *Water science and technology* **2014**, *70* (3), 437−443.
(60) Sajjadi, H.; Modaressi, A.; Magri, P.; Domańska, U.; Sindt, M.; Mieloszynski, J.-L.; Mutelet, F.; Rogalski, M. Aggregation of nanoparticles in aqueous solutions of ionic liquids. *J. Mol. Liq.* **2013**, *186*, 1−6.
(61) Petosa, A. R.; Brennan, S. J.; Rajput, F.; Tufenkji, N. Transport of two metal oxide nanoparticles in saturated granular porous media: role of water chemistry and particle coating. *Water research* **2012**, *46* (4), 1273−1285.
(62) French, R. A.; Jacobson, A. R.; Kim, B.; Isley, S. L.; Penn, R. L.; Baveye, P. C. Influence of ionic strength, pH, and cation valence on aggregation kinetics of titanium dioxide nanoparticles. *Environ. Sci. Technol.* **2009**, *43* (5), 1354−1359.
(63) Zhang, Y.; Gutierrez, L.; Benedetti, M. F.; Croué, J. P. Impact of electrolyte and natural organic matter characteristics on the aggregation and sedimentation of polystyrene nanoplastics. *Sci. Total Environ.* **2024**, *955*, No. 177131.
(64) Daneshfar, R.; Soulgani, B. S.; Ashoori, S. Identifying the mechanisms behind the stability of silica nano-and micro-particles: effects of particle size, electrolyte concentration and type of ionic species. *J. Mol. Liq.* **2024**, *397*, No. 124059.
(65) Gao, J.; Yu, F.; Zhang, P.; Wu, Z.; Liu, H.; Weiping, L. Distribution characteristics of TiO2 NPs in Daihai Lake and their stability regulated by abiotic factors. *Environ. Res.* **2024**, *263*, No. 120203.
(66) McHedlov-Petrossyan, N. O.; Kamneva, N. N.; Al-Shuuchi, Y. T. M.; Marynin, A. I. Interaction of C60 aggregates with electrolytes in acetonitrile. *Colloids Surf., A* **2017**, *516*, 345−353.
(67) Abdullah, M.; Low, G. K. C.; Matthews, R. W. Effects of common inorganic anions on rates of photocatalytic oxidation of organic carbon over illuminated titanium dioxide. *J. Phys. Chem.* **1990**, *94* (17), 6820−6825.
(68) Liang, H.-C.; Li, X.-Z.; Yang, Y.-H.; Sze, K.-H. Effects of dissolved oxygen, pH, and anions on the 2, 3-dichlorophenol degradation by photocatalytic reaction with anodic TiO2 nanotube films. *Chemosphere* **2008**, *73* (5), 805−812.
(69) Piscopo, A.; Robert, D.; Weber, J. V. Influence of pH and chloride anion on the photocatalytic degradation of organic compounds: Part I. Effect on the benzamide and para-hydroxybenzoic acid in TiO2 aqueous solution. *Applied Catalysis B: Environmental* **2001**, *35* (2), 117−124.
(70) Chen, L.; Li, X.; Zhang, J.; Fang, J.; Huang, Y.; Wang, P.; Ma, J. Production of hydroxyl radical via the activation of hydrogen peroxide by hydroxylamine. *Environ. Sci. Technol.* **2015**, *49* (17), 10373−10379.
(71) Antonopoulou, M.; Karagianni, P.; Konstantinou, I. K. Kinetic and mechanistic study of photocatalytic degradation of flame retardant Tris (1-chloro-2-propyl) phosphate (TCPP). *Applied Catalysis B: Environmental* **2016**, *192*, 152−160.
(72) Tee, S. Y.; Kong, J.; Koh, J. J.; Teng, C. P.; Zu Wang, X.; Wang, X.; Teo, S. L.; Thitsartarn, W.; Han, M.-Y.; Seh, Z. W. Structurally and surficially activated TiO2 nanomaterials for photochemical reactions. *Nanoscale* **2024**, *16*, 18165−18212.
(73) Carrier, M.; Guillard, C.; Besson, M.; Bordes, C.; Chermette, H. Photocatalytic degradation of diuron: experimental analyses and simulation of HO radical attacks by density functional theory calculations. *J. Phys. Chem. A* **2009**, *113* (22), 6365−6374.
(74) Koppaka, A.; Kirkland, J. K.; Periana, R. A.; Ess, D. H. Experimental Demonstration and Density Functional Theory Mechanistic Analysis of Arene C−H Bond Oxidation and Product Protection by Osmium Tetroxide in a Strongly Basic/Nucleophilic Solvent. *Journal of Organic Chemistry* **2022**, *87* (21), 13573−13582.
(75) Liu, Q.; Liggio, J.; Li, K.; Lee, P.; Li, S.-M. Understanding the impact of relative humidity and coexisting soluble iron on the OH-initiated heterogeneous oxidation of organophosphate flame retardants. *Environ. Sci. Technol.* **2019**, *53* (12), 6794−6803.
(76) Garbou, A. M.; Liu, M.; Zou, S.; Yestrebsky, C. L. Degradation kinetics of hexachlorobenzene over zero-valent magnesium/graphite in protic solvent system and modeling of degradation pathways using density functional theory. *Chemosphere* **2019**, *222*, 195−204.
(77) Sui, Q.; Gebhardt, W.; Schörder, H. F.; Zhao, W.; Lu, S.; Yu, G. Identification of new oxidation products of bezafibrate for better understanding of its toxicity evolution and oxidation mechanisms during ozonation. *Environ. Sci. Technol.* **2017**, *51* (4), 2262−2270.
(78) Tay, K. S.; Madehi, N. Ozonation of ofloxacin in water: by-products, degradation pathway and ecotoxicity assessment. *Sci. Total Environ.* **2015**, *520*, 23−31.
(79) Geleta, T. A.; Tee, R. Q.; Shih, Y.-H.; Chen, W.-L. Exploring charge transfer and degradation mechanism of one-step synthesized modified g-C3N4 for efficient photocatalytic bisphenol A removal under visible light. *Colloids Surf., A* **2025**, *719*, No. 136990.